Asian Journal of Chemistry; Vol. 37, No. 11 (2025), 2839-2845
ASIAN JOURNAL OF CHEMISTRY
https://doi.org/10.14233/ajchem.2025.34369

In vitro Antibacterial Activity and Dye Effluent Treatment Potential of Silver Nanoparticles Synthesized with *Paspalum vaginatum* Extract

HENRY U. ANUFORO[1,*], CAMPBELL O. AKUJOBI[2], NNEAMAKA A. CHIEGBOKA[1], OLUSOLA O. IBEH[3], ENUMA E. MIKE-ANOSIKE[2], LAWRENCIA A. ADJEROH[1], AUGUSTA A. NWACHUKWU[4] and ETHELBERT U. EZEJI[4]

[1]Department of Biology, School of Biological Sciences, Federal University of Technology, PMB 1526, Owerri, Nigeria
[2]Department of Microbiology, School of Biological Sciences, Federal University of Technology, PMB 1526, Owerri, Nigeria
[3]Department of Forensic Science, School of Biological Sciences, Federal University of Technology, PMB 1526, Owerri, Nigeria
[4]Department of Biotechnology, School of Biological Sciences, Federal University of Technology, PMB 1526, Owerri, Nigeria

*Corresponding author: E-mail: henry.anuforo@futo.edu.ng

Received: 1 July 2025 *Accepted*: 7 October 2025 *Published online*: 27 October 2025 AJC-22174

Paspalum vaginatum vastly grows in the Southeastern region of Nigeria, but without major known applications. After GC-MS analysis, aqueous extract of its aerial parts of *P. vaginatum* was employed in silver nanoparticles (AgNPs) biosynthesis. Chromatogram revealed 10 bioactive components in the extract. The synthesized AgNPs exhibited a characteristic UV-Vis absorbance peak at 320 nm, confirming their surface plasmon resonance. Fourier-transform infrared (FTIR) analysis revealed the presence of functional groups such as O–H and N–H stretching, O=C=O stretching and C≡C stretching, suggesting the involvement of biomolecules in nanoparticle stabilization and reduction. Furthermore, X-ray diffraction (XRD) analysis showed prominent peaks at 2θ values of 28.98º, 34.22º, 37.98º, 44.28º and 64.46º, corresponding to the face-centered cubic (FCC) crystalline structure of AgNPs, while dynamic light scattering (DLS) and transmission electron microscopy (TEM) analyses indicated particle sizes of 11.51 ± 2.53 nm (PDI: 0.60) and 3.41 ± 1.60 nm, respectively, highlighting the presence of well-dispersed, nanoscale particles with moderate polydispersity. There were 19.00 ± 2.16 mm and 15.00 ± 2.85 mm zones of inhibition of *Escherichia coli* and *Salmonella* sp. growth at 53.3 µg/mL concentration of AgNPs. At 1.72 mg/mL of AgNPs, the percentages of methylene blue and safranin effluent treatment were 37.14 ± 1.63% and 33.76 ± 2.37% after 1 h, 40.38 ± 0.13% and 46.47 ± 1.04% after 2 h and 48.45 ± 0.88% and 53.48 ± 1.13% after 3 h of solar irradiation. These findings demonstrate that the AgNPs synthesized using *P. vaginatum* extract possess favourable physico-chemical characteristics, which contribute to their appreciable biological and photocatalytic activities.

Keywords: Photocatalytic degradation, Effluent treatment, Antibacterial activity, *Paspalum vaginatum*, Silver nanoparticles.

INTRODUCTION

The remarkable physico-chemical characteristics of metallic nanoparticles have made them useful in a variety of applications such as cellular transportation, synthetic biology and health care [1]. Silver nanoparticles (AgNPs) in particular have been identified as viable antibacterial agent for the future, due to their potent antibacterial qualities. In view of their strong positive reducing capacity, AgNPs are thermodynamically unfavourable when oxidized [2]. Hence AgNPs are very stable in alcoholic and aqueous solutions and don't require sealing agents [3]. This has led to their successful application in various medical goods, including contact lenses, coating materials for catheters used for the drainage of cerebrospinal fluid and other medical devices [1]. Furthermore, they have been utilized in wound dressings, surgical masks, bone cement, impregnated textile fabrics, nanogels and nanolotions [4]. In fact, large numbers of silver-based products have been approved by international regulatory agencies and are currently being marketed [1].

Numerous techniques have been used to synthesize these metal nanoparticles [5]. The biological process is a green method of nanoparticles synthesis with the advantage of reduced environmental and human toxicity. This is because the biological synthesis approach produces nanoparticles using enzymes, microbes, plants or plant extracts instead of chemicals as obtains in chemical and physical approaches [5,6]. Compared to the physical and chemical approaches, green synthesis is more ecologically friendly, uses less energy, is less expensive,

can be produced in large quantities and is more efficient [7,8]. When compared to other organisms used in biological method, the utilization of plants produces more stable nanoparticles at a faster rate of synthesis [7,9]. Flavonoids, terpenoids, ketones, amides, aldehydes and carboxylic acids are the primary phytochemicals found in plant extracts. While serving as capping agents, these phytochemicals also reduce metal ions to develop their corresponding nanoparticles [10]. In some earlier researches, extracts of *Euphorbia confinalis* and *Scelocarrya birrea* [11], *Prunus dulcis* and *Mangifera indica* [12] and *Vernonia amygdalina* [13] were used to prepare silver nanoparticles. Thorough analysis reveals that a large number of earlier investigations involved extracts of plants with significant ecological, medical or economic benefits. It is believed that the overexploitation of these plants may result in their extinction in the near future. Consequently, focus should be directed toward other underutilized species such as *Paspalum vaginatum*, which was used in the present study.

Paspalum vaginatum (seashore paspalum) is a temperate perennial grass commonly found in tropical and subtropical regions [14]. In the 1700s and 1800s, it was utilized as bedding in trading ships that traveled between Africa, North and South America, Central America and the Caribbean Islands [15]. In addition, *P. vaginatum* has been extensively utilized for animal feed, dredge material and sand dune stabilization, coastal wetland restoration and salt-affected land rehabilitation. Because of its wide range of ecological tolerances and life history characteristics, *P. vaginatum* is well established and useful to land and resource managers around the world. It is a rhizomatous, stoloniferous, mat-forming perennial grass that is ecologically aggressive and frequently grows in large colonies. These allowed it to change the function of wetland ecosystems, colonize disturbed, barren or ephemeral soil deposits early and successfully and, once established, dispense with native species. These features make it an invasive species [14].

EXPERIMENTAL

All the chemicals including silver nitrate, sodium hydroxide, hydrochloric acid, microbiological media, dye samples and other reagents were purchased from the commercial chemicals suppliers and used without any purification.

Samples collection and preparation: *Paspalum vaginatum* is vastly available in the Southeastern region of Nigeria and has less known application. Insecticide-free, fresh aerial parts of *P. vaginatum* were collected from the botanical garden of the Forestry and Wildlife Technology (FWT) Department, at the Federal University of Technology, Owerri (FUTO), Nigeria. After validation by a taxonomist at the Department, it was assigned the voucher number FUTO/FWT/ERB/2024/108 and deposited in their herbarium. The samples were carefully sorted, washed under running tap, sundried and milled into powders. Preparation of aqueous extract was carried out by boiling 107 g of powdered plant sample with 1,500 mL of distilled water for 20 min. After cooling, it was filtered using Whatman No. 1 filter paper and the filtrate was preserved in the refrigerator. Concentration of the extract was determined by completely evaporating 10 mL of extract, in triplicates and calculating the average weight of the resulting powder [12].

Gas chromatographic-mass spectrometry (GC-MS) analysis: GC-MS analysis of phytochemical compositions of *P. vaginatum* extract was done using Thermo-Scientific GC Focus Series DSQ. Helium gas served as the carrier gas and was maintained at a constant flow rate of 1 mL per min with 1 μL infection volume. The hot oven and injector were kept at temperatures of 110 ºC and 250 ºC, respectively, with 10 ºC per min increase rate up to 200 ºC, followed by 5 ºC per min up to 280 ºC. Closing temperature was maintained at 280 ºC after 9 min. After eluting peaks of different compounds from the GC column, their retention times were recorded. Resulting data were compared to mass spectra of known compounds and searched on the MS database of similar compounds with the same retention time and molecular mass [16].

Biogenic preparation of silver nanoparticles: The temperature of 10 mL of prepared aqueous extract of *P. vaginatum* and 90 mL of $AgNO_3$ solution, used as precursor, was increased to 80 ºC using water bath. Then the solution was gently added into the extract in a 250 mL conical flask. After 3 h of continuous stirring, synthesis was allowed to continue overnight in a dark. Change in colour of the mixture on addition of $AgNO_3$ solution was visually monitored. Thereafter, the resulting AgNPs suspension was centrifuge at 5,000 rpm for 20 min. After discarding the supernatant, the AgNPs pellets were washed thrice with distilled water to remove impurities. The pellets were finally dried in an oven at 50 ºC and stored in the airtight container [17].

Characterization: The UV-Visible spectrophotometer (Shimadzu UV-1780) was employed to measure the wavelength of maximum absorption (λ_{max}) of the synthesized AgNPs. As well, the UV-Vis spectrum of the nanoparticles was measured by scanning the wavelength range of 200-800 nm. The particle size was determined using a particle size analyzer (PSA) (Biobase BK 802N). X-ray diffractometer (X-Ray Diffraction Rigaku Miniflex 600) and transmission electron microscope (JEM 2100F (JEOL, Tokyo, Japan) were used to determine the structure, morphology and composition of the AgNPs [17]. Fourier transform infrared (FTIR) spectroscopy (Bruker FTIR Spectrometer ALPHA II) in the diffuse reflectance mode at a resolution of 4 cm^{-1} in KBr pellets was employed to ascertain the nature of various functional groups constituents of the extract. Malvern Zen 3600 instrument was used to determine the size distribution (dynamic light scattering) of nanoparticles in a solution.

***In vitro* antibacterial analysis:** The method of Shaik *et al.* [1] was adopted with minor adjustment, to evaluate the antibacterial activity of the AgNPs. Clinical isolates of known waterborne pathogens, *Escherichia coli* and *Salmonella* sp, were obtained from the Diagnosis Unit of the FUTO Teaching Hospital, Owerri, Nigeria. After sub-culturing, revalidation of *Salmonella* sp. isolates was done by inoculating it on xylose-lysine-deoxycholate agar (XLD, Oxoid, UK) and Salmonella-Shigella agar (SSA). The formation of colourless colonies with black centres on SSA and red-pink colonies of about 2 to 3 mm in diameter, with black centres on XLD agar were taken as preliminarily positive for *Salmonella* sp [18]. Conversely, *E. coli* was revalidated by inoculating on eosin methylene blue (EMB) agar and observing after 24 h of incubation. The form-

ation of colonies having metallic sheen colouration with black centre was considered as positive test for *E. coli* [19].

First, a loopful of each identified isolate was inoculated into 5 mL of nutrient broth and incubated for 24 h, at 37 ºC, to revive the cultures. The turbidity of each inoculum was adjusted to match 0.5 McFarland solution (~10^8 cfu/mL) using spectrophotometric method. Then 0.1 mL of each standardized inoculum was aseptically spread onto prepared Mueller-Hinton (MH) agar plates. Wells were aseptically bored into the plates and few drops of each 53.3 µg/mL, 26.7 µg/mL and 13.3 µg/mL concentration of synthesized AgNPs were used to fill appropriate wells as labeled. Also, drops of sterilized distilled water and ciprofloxacin disc were applied as negative and positive controls, respectively. After allowing the treatments to permeate the media, plates were incubated at 37 ºC for 24 h. Afterward, observed diameter of growth inhibition zones were recorded for each concentration and bacterium. The experiments were conducted in duplicates.

Wastewater treatment procedure: The wastewater treatment potential of the synthesized AgNPs was separately studied by determining its photocatalytic activity against 0.5 mg/L solution of each of methylene blue and safranin, under solar irradiation. Each experiment was set up with 30 mL each of the dye wastewaters and final AgNPs concentrations of 1.72 mg/mL, 0.86 mg/mL and 0.43 mg/mL. After thorough mixing in the dark, the mixtures were exposed to intense solar irradiation. At 0, 60, 120 and 180 min of exposure, aliquots of each treatment were carefully collected after stirring and then centrifuged for 20 min, at 4000 rpm, to remove AgNPs photocatalysts. The absorbance of each supernatant was read using UV visible absorbance at 668 nm for methylene blue and 513 nm for safranin. Control experiments were also conducted in duplicates with no addition of AgNPs. Percentage dye degradation at the intervals of solar irradiation was calculated using eqn. 1:

$$\text{Wastewater treatment } (\%) = \frac{A_o - A_t}{A_o} \times 100 \qquad (1)$$

where A_o refers to the initial absorbance of wastewater sample and A_t is the absorbance of wastewater after t min of solar irradiation [20].

Statistical analysis: Microsoft Excel 2010 was used for data entry, formatting and plotting of charts. Appropriate tools in Microsoft Excel 2010 were used to compute the mean and standard deviations of resulting datasets. Minitab 17 software was used to compute the analysis of variance and least significant differences (at $\alpha = 0.05$) where necessary. Sigma Plot® was used to model the datasets for wastewater treatment.

RESULTS AND DISCUSSION

The concentration of the prepared *P. vaginatum* extract was 7.33 ± 1.89 mg/mL with a pH of 6.5 ± 0.9. The GC-MS chromatogram of extract of *P. vaginatum* revealed 10 bioactive components. The retention time, molecular formula and molecular weights of the phytochemical components are shown in Table-1. The phytochemicals are involved in the reduction and capping of silver ions to form silver nanoparticles.

UV-visible spectra: On addition of $AgNO_3$ into the extract, it was observed that colour of the mixture changed from light brown to deep brown which continued to deepen as time progressed. Fig. 1 shows the absorbance spectrum of the AgNPs obtained in this study with *P. vaginatum* extract, using UV-visible spectrophotometer. The spectrum showed broad base between 289 nm and 514 nm, with a peak of absorbance observed at 320 nm.

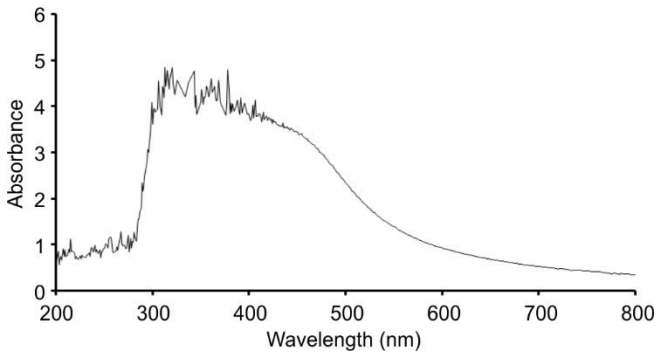

Fig. 1. Absorbance spectrum of AgNPs synthesized with *P. vaginatum* extract

Similar changes in colour of reacting mixtures have been visualized and reported in previous studies. Reports showed that the yellowish-green colour of reaction mixture changed to brown, signifying that ionic silver (Ag^+) was changed into metallic silver (Ag^0), which then self-assembled into AgNPs [5]. Furthermore, a change in colour from pale-yellow to dark-brown signified the formation of AgNPs from carrot

TABLE-1
DETAILS OF TEN STRUCTURES OBSERVED ON CHROMATOGRAM

Peak No.	Retention time (min)	Total (%)	Identity of compound	m.f.	m.w.
1	7.40	1.54	Hexadecanoic acid, methyl ester	$C_{17}H_{34}O_2$	270
2	7.69	3.27	*n*-Hexadecanoic acid	$C_{16}H_{32}O_2$	256
3	8.27	1.48	9-Octadecenoic acid (Z)-, methyl ester	$C_{19}H_{36}O_2$	296
4	8.54	5.03	Oleic acid	$C_{18}H_{34}O_2$	282
5	9.02	2.38	Dodecanoic acid, 1-(hydroxymethyl)-1,2-ethanediyl ester	$C_{27}H_{52}O_5$	456
6	9.43	3.45	N-[4-Methoxy-6-(2,2,2-trifluoro-1-trifluoromethyl-ethoxy)-[1,3,5]triazin-2-yl]-benzene-1,4-diamine	$C_{13}H_{11}F_6N_5O_2$	383
7	9.78	6.76	Benzenamine, 4-methoxy-N-(triphenylphosphoranylidene)	$C_{25}H_{22}NOP$	383
8	10.70	7.18	4-Nitrophenyl laurate	$C_{18}H_{27}NO_4$	321
9	10.23	1.87	Dodecanoic acid, 1,2,3-propanetriyl ester	$C_{39}H_{74}O_6$	638
10	14.94	1.01	4-Methoxy-3-nitrobenzyl alcohol	$C_8H_9NO_4$	183

extract [17]. The observed UV-vis bands which were due to surface plasmon resonance (SPR) absorption, confirmed the synthesis of AgNPs. The activation of free electrons usually results in SPR in nanoparticles [21].

FTIR spectral studies: The resulting FTIR spectra of *P. vaginatum* and AgNPs synthesized with its extract are shown in Fig. 2. For *P. vaginatum*, there are 12 major peaks for the AgNPs, among which were 6 strong peaks, 4 medium peaks and 2 weak peaks. The spectra, the peaks, their appearances, functional groups and compounds present, were identified as shown in Table-2.

An earlier study observed that the region between 4000 and 400 cm^{-1} showed some prominent peaks at 3337, 3009, 1743, 1091 and 733 cm^{-1}. These peaks were due to -C–O, C–H, C=C, CH_2 and O–H stretching vibrations respectively, in the AgNPs. These functional groups are constituents of reducing sugars, proteins, flavonoids and saccharides that are among the phytochemicals found in *Gomphrena serrate* tuber extract [22]. Similarly, results showed that transmission peaks for *Rosa chinensis* root extract were 3244, 2987, 2900, 1608, 1394, 1249, 1066, 879 and 670 cm^{-1}, while the transmission peaks for AgNPs from its root extract were 3197, 2987, 2900, 1543, 1394, 1249, 1066, 870 and 669 cm^{-1}. Also, its leaf extract produced peaks at 3255, 2972, 2900, 1608, 1394, 1242, 1045 and 879 cm^{-1}, while AgNPs synthesized utilizing the leaf extract produced peaks at 3230, 2987, 2900, 1608, 1394, 1242, 1066,179 and 669 cm^{-1}. The C–C stretch of alkenes or the C–O stretch of amides caused the band in FTIR at 1608 cm^{-1}. The presence of N–H and CO groups in the AgNPs were revealed by the wavelength change from 1608 to 1543 cm^{-1}. The 2987-2972 cm^{-1} range designated the aromatic C–H stretching band. Aliphatic amine group in proteins produced the peak at 1394 cm^{-1} ascribed to C–N stretching. The =CH group caused absorption in aromatic compounds at 650–880 cm^{-1}. The C-C stretching of an organic molecule in the plant extracts was demonstrated by the 1250-1020 cm^{-1} absorption bands [5].

XRD studies: Fig. 3 shows the XRD spectrum of the synthesized AgNPs, with diffraction peaks corresponding to (002), (111), (200) and (220) reflection planes of the face-centered cubic (fcc) structure. The 2θ lattice plane values were 28.98º, 34.22º, 37.98º, 44.28º and 64.46º. Using Scherrer's formula with diffraction angle (θ) of 44.28 and full width at half maximum (FWHM) (β) of the most intense diffraction peak that was detected to be 0.74, the crystalline size was estimated as 12.10 nm. The 2θ peak positions was specified with the JCPDS No.: 04-002-1347.

Report showed that AgNPs produced using extract of *Gomphrena serreta* have a face-centered cubic structure with (111), (002), (022) and (113) planes that can be corresponded to diffraction peaks at 2θ values of 38.13º, 46.72º, 64.44º and 76.93º. This confirmed the presence and high crystallinity of the silver nanoparticles. It added that due to the presence of organic compounds in the extract, the pattern of AgNPs generated from *G. serreta* extract displayed a few extra peaks [22]. The XRD pattern of the AgNPs synthesized using *R. chinensis* root extract revealed 4 strong peaks at (111), (200), (220) and (311) planes. These matched the face-centered cubic lattice structure which is characteristic of AgNPs and confirmed the

TABLE-2
DESCRIPTION OF PEAKS IN FTIR SPECTRUM OF AgNPs

Absorbance peak (cm^{-1})		Appearance	Fucntional group	Coumpound present
AgNPs	*P. vaginatum*			
3470.20		Broad	O-H stretching	Alcohol and phenols
		Medium	N-H stretching	Primary amines
	3309.9	Weak	N–H stretching	Secondary amine
3142.10		Strong	O-H stretching	Carboxylic acid
	2918.5	Strong	N–H stretching	Amine salt
2914.60	2851.4	Strong	O-H stretching	Carboxylic acid
2847.70		Strong	N-H stretching	Amine salt
2355.70		Medium	O=C=O stretching	Carbon dioxide
2113.40		Weak	C≡C stretching	Alkyne
1990.40		Weak	C-H bending	Aromatic compound
	1729.5	Weak	C=O stretching	Aldehyde
1602.80	1591.6	Strong	N-H bending	Amine

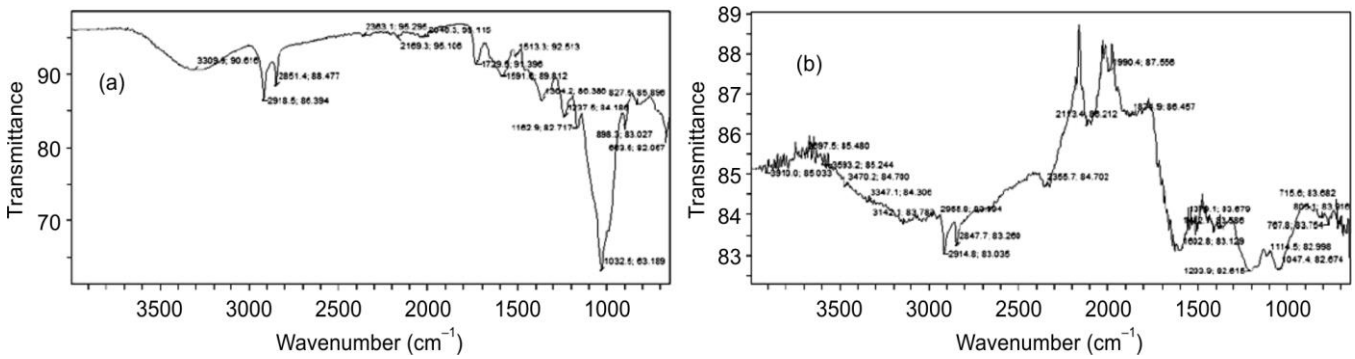

Fig. 2. FTIR spectrum of (a) *P. vaginatum* extract (b) AgNPs synthesized with *P. vaginatum* extract

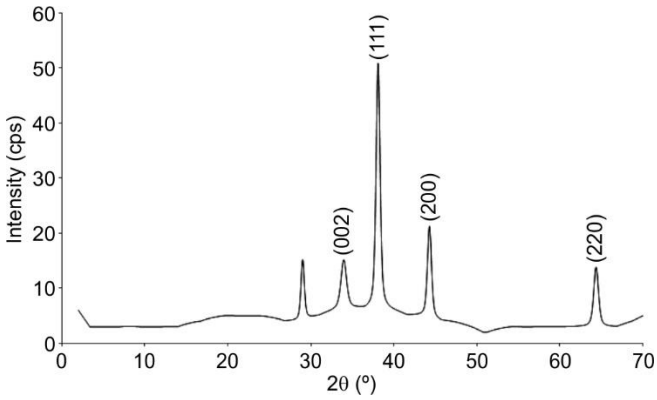

Fig. 3. XRD spectrum of AgNPs synthesized with *P. vaginatum* extract

efficient synthesis and crystalline nature of resulting silver nanoparticles. Their Bragg's reflection (2θ) = 38.30º, 44.41º, 64.59º and 77.50º. Debye-Scherer method was employed and results showed that the average crystalsize of AgNPs from *R. chinensis* root extract was 13.39 nm [5]. This is similar to the size of AgNPs synthesized in the present study.

DLS studies: Results of dynamic light scattering (DLS) revealed that the size of biosynthesized AgNPs in this study was 11.51 ± 2.53 nm, with polydispersity index (PDI) of 0.60. The AgNPs were non-uniform, polydispersed and non-agglomerated in solution. The polydispersity index (PDI), ranging from 0 to 1, indicates particle size distribution, where values near 0 reflect a monodisperse system, while those approaching 1 signify a poly-disperse or heterogeneous distribution [23]. Monodisperse silver nanoparticles have better application capabilities compared to polydisperse forms. The PDI value of less than 0.3 indicates that monodisperse nanoparticles are formed [5].

TEM studies: The transmission electron micrograph obtained at 20 nm resolutions for AgNPs is shown in Fig. 4. It revealed that their sizes ranged from 0.52 nm to 5.32 nm, with an average of 3.41 ± 1.60 nm. The AgNPs were majorly spherical in morphology, with no agglomeration. The light, darkest and darker phases of the nanoparticles were also revealed by TEM images.

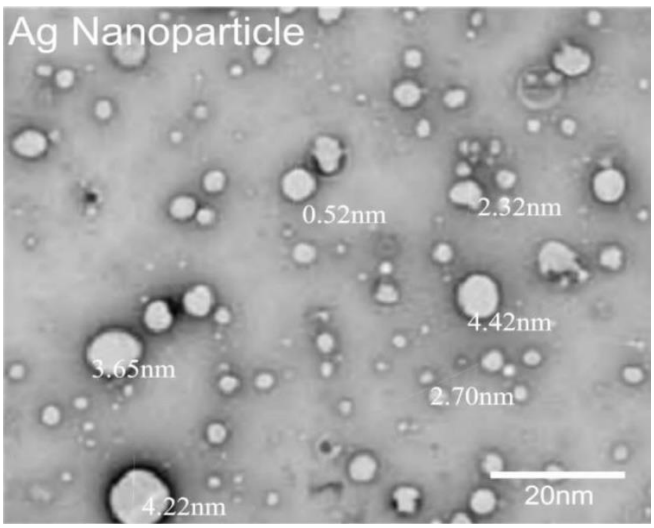

Fig. 4. Micrograph showing sizes and shapes of AgNPs synthesized with *P. vaginatum* extract at 20 nm resolutions

Antibacterial activity: Fig. 5 presents the antibacterial activities, measured by zones of growth inhibitions, of different concentrations of AgNPs and other control treatments. *E. coli* showed higher sensitivity to AgNPs than *Salmonella* sp. There were 19.00 ± 2.16 mm, 14.70 ± 2.05 mm and 11.00 ± 2.16 mm zones of inhibitions of *E. coli* growth, as well as 15.00 ± 2.85 mm, 11.00 ± 3.48 mm and 9.30 ± 2.25 inhibition of *Salmonella* sp. growth, at 53.3, 26.7 and 13.3 µg/mL AgNPs concentrations respectively. Ciprofloxacin produced the highest ZOI in both isolates. However, there was no significant difference in the sensitivities of the isolates to AgNPs.

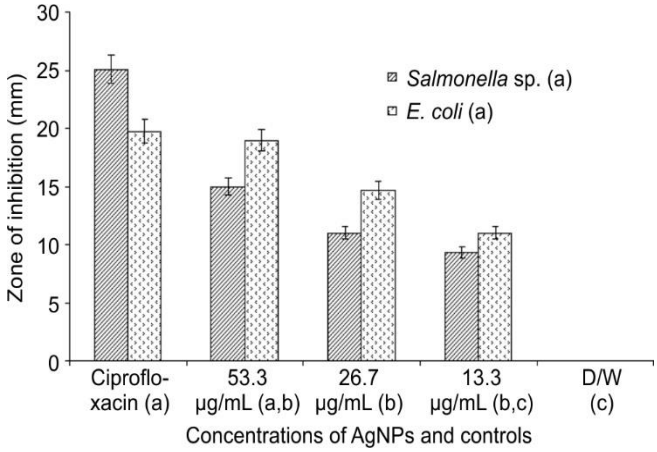

Fig. 5. Zones of inhibition of bacterial growths at different concentrations of AgNPs synthesized with *P. vaginatum* extract. Samples with similar lower case letters, in parenthesis, are not significantly different

Wastewater treatment potential of synthesized AgNPs

Treatment of methylene blue wastewater: Fig. 6 shows the percentage photocatalytic degradation of methylene blue dye wastewater by AgNPs synthesized with *P. vaginatum* extract. At 1.72 mg/mL of nanoparticles, the percentage wastewater treatment was 37.14 ± 1.63% at 1 h, 40.38 ± 0.13% at 2 h and 48.45 ± 0.88% at 3 h. It reduced to 17.17 ± 1.29% at 1 h, 27.05 ± 3.99% at 2 h and 29.87 ± 1.89% at 3 h, when the concentration of AgNPs was reduced to 0.43 mg/mL. Control samples recorded appreciably lower reduction in concentration of the dye, with 5.07 ± 1.68% at 1 h, 7.49 ± 1.28% at 2 h and 9.56 ± 0.29% at 3 h due to photolysis. The percentage degradation of methylene blue dye by AgNPs at 1.72 mg/mL concentration was significantly different from its percentage degradation at lower concentrations studied, as well as the control. Modeling showed that the wastewater treatment potential of AgNPs at 1.72 mg/mL concentration on 0.5 mg/mL methylene blue dye was best described by the polynomial quadratic equation (eqn. 2):

$$f = y_0 + ax + bx^2; \text{ with } R^2 = 1 \quad (2)$$

where f is the percentage degradation of methylene blue dye wastewater, x is duration of treatment (h), y_0 = 38.73, a = -4.00 and b = 2.41.

Treatment of safranin wastewater: At 1.72 mg/mL concentration, synthesized AgNPs recorded 33.76 ± 2.37% dye degradation after 1 h, 46.47 ± 1.04% after 2 h and 53.48 ± 1.13% after 3 h of exposure to solar irradiation. At 0.43 mg/mL, percentage degradation also reduced to 12.20 ± 2.00% after

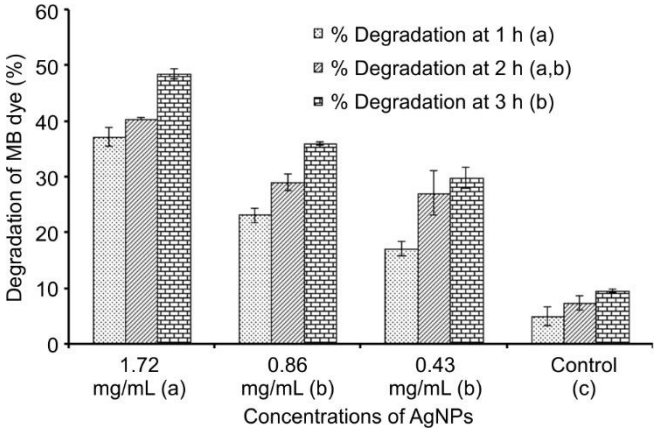

Fig. 6. Percentage degradation of methylene blue dye at different concentrations of AgNPs photocatalyst over 3 h. Samples with different lower case letters in parenthesis, are significantly different ($\alpha = 0.05$)

1 h, 15.34 ± 2.42% after 2 h and 23.53 ± 2.89% after 3 h of exposure. These were considerably higher than 5.14 ± 0.92% after 1 h, 6.30 ± 0.79% after 2 h and 8.79 ± 0.76% degradation recorded in control samples due to photolysis (Fig. 7). Analysis revealed that percentage degradation recorded at the various concentrations were significantly different from each other and that of control samples. Modelling of results indicated that photocatalytic activity of 1.72 mg/mL concentration of synthesized AgNPs on 0.5 mg/mL safranin dye, was best described by the polynomial quadratic equation (eqn. 3):

$$f = y_0 + ax + bx^2, \text{ with } R^2 = 1 \quad (3)$$

where f is percentage degradation of safranin dye solution, x is duration of exposure (h), $y_0 = 15.33$, a = 21.28 and b = -2.86.

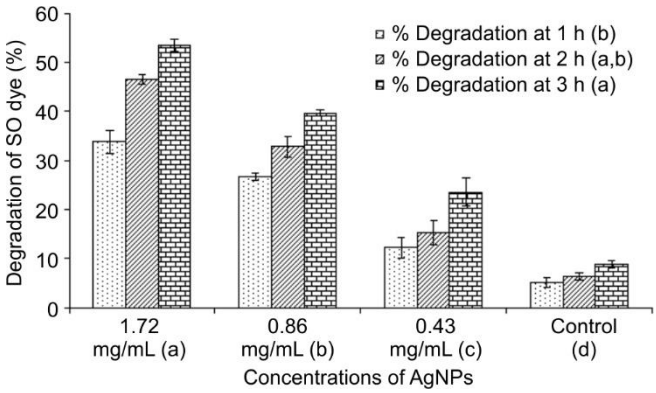

Fig. 7. Percentage degradation of safranin dye at different concentrations of AgNPs photocatalyst, over 3 h. Samples with different lower case letters in parenthesis, are significantly different ($\alpha = 0.05$)

In this study, the prepared silver nanoparticles showed greater potential in treating wastewater containing safranin dye compared to wastewater containing methylene blue dye. This may be attributed to differences in their structures. The results indicated that prolonged solar irradiation of the wastewater enhanced the percentage of effluent treatment, with a gradual decrease in dye concentration observed over time. A related study had shown that treatment with biosynthesized AgNPs led to a visible shift toward higher wavelengths and a marked reduction in methylene blue absorbance, demonstrating effective dye degradation. The reaction was completed within 20 min, resulting in complete decolorization of methylene blue. This was accompanied by an increase in the surface plasmon resonance (SPR) peak of AgNPs at 664 nm alongside a significant decrease in methylene blue absorbance [24]. In another study that used silver nanoparticles made from honey to catalyze the degradation of methylene blue, it was observed that after 72 h, 92% of the methylene blue had been degraded. On analyzing the samples with HPLC, a number of additional peaks emerged indicating the formation of byproducts of the photocatalysis [25]. Moreover, a study on the breakdown of methylene blue dye using AgNPs made from extract from *Andographis paniculata* leaves revealed that the degradation effectiveness of AgNPs was 84% after 16 h of exposure. The proportion of methylene blue dye degraded under sunlight increased with duration of dye exposure [26].

Conclusion

The results obtained from characterization revealed that silver nanoparticles were successfully synthesized using *P. vaginatum* extract. The GC-MS characterization of the extract showed 10 phytochemicals in the extract. Results indicated that at 1.72 mg/mL of silver nanoparticles, the percentage of methylene blue effluent treatment was 37.14 ± 1.63% after 1 h, 40.38 ± 0.13% after 2 h and 48.45 ± 0.88% after 3 h. For safranin effluent, the percentage treatment recorded was 33.76 ± 2.37% after 1 h, 46.47 ± 1.04% after 2 h and 53.48 ± 1.13% after 3 h of solar irradiation. Thus, safranin was more sensitive to treatment with silver nanoparticles than methylene blue. It was also observed that the percentage of effluents treatment increased with increasing duration of solar irradiation. For *in vitro* antibacterial activity of synthesized silver nanoparticles, *E. coli* showed higher sensitivity to AgNPs than *Salmonella* sp. It was 19.00 ± 2.16 mm, 14.70 ± 2.05 mm and 11.00 ± 2.16 mm zones of inhibitions of *E. coli* growth, as well as 15.00 ± 2.85 mm, 11.00 ± 3.48 mm and 9.30 ± 2.25 inhibition of *Salmonella* sp. growth, at 53.3, 26.7 and 13.3 μg/mL AgNPs concentrations respectively.

ACKNOWLEDGEMENTS

The authors acknowledge the support of the Heads of Departments of Biology and Biotechnology for granting them access to their facilities used for this study.

CONFLICT OF INTEREST

The authors declare that there is no conflict of interests regarding the publication of this article.

REFERENCES

1. M. Shaik, M. Khan, M. Kuniyil, A. Al-Warthan, H. Alkhathlan, M. Siddiqui, J. Shaik, A. Ahamed, A. Mahmood, M. Khan and S. Adil, *Sustainability*, **10**, 913 (2018); https://doi.org/10.3390/su10040913.
2. S.-H. Jeon, P. Xu, N. H. Mack, L. Y. Chiang, L. Brown and H.-L. Wang, J. Phys. Chem. C, **114**, 36 (2010); https://doi.org/10.1021/jp907757u
3. P. Mathur, S. Jha, S. Ramteke and N. Jain, *Artif. Cells Nanomed. Biotechnol.*, **46(sup1)**, 115 (2018); https://doi.org/10.1080/21691401.2017.1414825

4. B.S. Atiyeh, M. Costagliola, S.N. Hayek and S.A. Dibo, *Burns*, **33**, 139 (2007); https://doi.org/10.1016/j.burns.2006.06.010
5. M. Bhusal, I. Pathak, A. Bhadel, D.K. Shrestha and K.R. Sharma, *Heliyon*, **10**, e33603 (2024); https://doi.org/10.1016/j.heliyon.2024.e33603
6. N. Liaqat, N. Jahan, Khalil-ur-Rahman, T. Anwar and H. Qureshi, *Front. Chem.*, **10**, 952006 (2022); https://doi.org/10.3389/fchem.2022.952006
7. H.U. Anuforo, T.E. Ogbulie, A.C. Udebuani and E.U. Ezeji, *J. Microbiol. Res.*, **8**, 74 (2023); https://doi.org/10.47430/ujmr.2382.009
8. M.G. Savvidou, E. Kontari, S. Kalantzi and D. Mamma, *Materials*, **17**, 187 (2024); https://doi.org/10.3390/ma17010187
9. S. Iravani and B. Zolfaghari, *BioMed Res. Int.*, **2013**, 639725 (2013); https://doi.org/10.1155/2013/639725
10. T.C. Prathna, N. Chandrasekaran, M.A. Raichur and A. Mukherjee, *Colloids Surf. B Biointerfaces*, **82**, 152 (2011); https://doi.org/10.1016/j.colsurfb.2010.08.036
11. N. Mukaratirwa-Muchanyereyi, C. Gusha, M. Mujuru, U. Guyo and S. Nyoni, *Results Chem.*, **4**, 100402 (2022); https://doi.org/10.1016/j.rechem.2022.100402
12. N.D. Hai, N.M. Dat, L.M. Huong, L.T. Tai, D.B. Thinh, N.T.H. Nam, N.T. Dat, M.T. Phong and N.H. Hieu, *Colloids Surf. B*, **220**, 112974 (2022); https://doi.org/10.1016/j.colsurfb.2022.112974
13. M. Tesfaye, Y. Gonfa, G. Tadesse, T. Temesgen and S. Periyasamy, *Heliyon*, **9**, e17356 (2023); https://doi.org/10.1016/j.heliyon.2023.e17356
14. M. Ramadan, F. Hassan, M.I. Fetouh and R. Selim, *J. Sustain. Agric. Environ. Sci.*, **4**, 68 (2025); https://doi.org/10.21608/jsaes.2025.425331.1181
15. R.R. Duncan and R.N. Carrow, Seashore paspalum: the environmental turfgrass, John Wiley & Sons, Inc., Hoboken, NJ, USA (1999).
16. S. Sadiqi, M. Hamza, F. Ali, S. Alam, Q. Shakeela, S. Ahmed, A. Ayaz, S. Ali, S. Saqib, F. Ullah and W. Zaman, *Molecules*, **27**, 6281 (2022); https://doi.org/10.3390/molecules27196281
17. N. Pramasari, A.G. Anjani, F.A. Muslikh, T.P. Lestari and F. Shoviantari, *Nat. Prod. Res.*, **8**, 12 (2024); https://doi.org/10.26538/tjnpr/v8i12.35
18. S. Abdul and A. Ferhat, *Rom. Biotechnol. Lett.*, **24**, 2 (2019).
19. https://asm.org/protocols/eosin-methylene-blue-agar-plates-protocol#:~:text=EMB%20agar%20is%20also%20used,gram%2Dnegative%20bacteria%20appear%20pink
20. P. Peerakiatkhajohn, T. Butburee, J.H. Sul, S. Thaweesak and J.H. Yun, *Nanomaterials*, **11**, 1059 (2021); https://doi.org/10.3390/nano11041059
21. E.K. Kambale, C.I. Nkanga, B.P.I. Mutonkole, A.M. Bapolisi, D.O. Tassa, J.M.I. Liesse, R.W.M. Krause and P.B. Memvanga, *Heliyon*, **6**, e04493 (2020); https://doi.org/10.1016/j.heliyon.2020.e04493
22. A. Cherukuri and P.R. Kammela, *J. Sci. Res.*, **66**, 358 (2022); https://doi.org/10.37398/JSR.2022.660138
23. J.I. Seeman, *ACS Omega*, **7**, 1 (2022); https://doi.org/10.1021/acsomega.1c04845
24. C.K. Githala, S. Raj, A. Dhaka, S.C. Mali and R. Trivedi, *Front. Chem.*, **10**, 994721 (2022); https://doi.org/10.3389/fchem.2022.994721
25. M.I. Al-Zaban, M.A. Mahmoudb and M.A. AlHarbi, *Saudi J. Biol. Sci.*, **28**, 2007 (2021); https://doi.org/10.1016/j.sjbs.2021.01.003
26. S.S. Noorafsha, K. Anil, K. Anupama, V. Damini and M. Anju, *J. Pharm. Res. Int.*, **33**, 47B (2021); https://doi.org/10.9734/jpri/2021/v33i47B33103